2013 IEEE/RSJ International Conference on
Intelligent Robots and Systems (IROS)
November 3-7, 2013. Tokyo, Japan

Longitudinal Slip versus Skid of Planetary Rovers' Wheels Traversing on Deformable Slopes*

Liang Ding, *Member, IEEE* , Haibo Gao, Zongquan Deng, Junlong Guo, Guangjun Liu, *Senior Member, IEEE*

Abstract— **The wheels of planetary rovers will slip when they climbs up deformable slopes. On the contrary, the wheels will skid in the longitudinal direction in order to generate resistance force to balance the gravity component when a rover moves down the slopes. The wheel-terrain interaction principles of slip versus skid are quite different, but there is little research about the longitudinal skid mechanics and the relationship of it with the slip mechanics. This paper analyzes the problem of longitudinal slip and skid that occur to a wheel on the slopes with the knowledge of terramechanics. The slip and skid mechanics are compared based on experimental results measured by a single wheel testbed. The piece wise linear function is proposed to predict the drawbar pull and resistance moment under both slip and skid conditions. A semi-empirical equation of predicting the skid mechanics according to the slip mechanics is also provided. The models are verified using the experimental data.**

I. INTRODUCTION

The planetary rovers including those for the exploration of the Mars [1-3] and the moon [4] are required to traverse on challenging terrains to achieve their scientific goals such as investigating the origin of the solar system and looking for evidence of life. During the recent years, the wheel-terrain interaction mechanics has been applied to the development of wheeled mobile robots (WMRs), in particular to the planetary exploration rovers, as it is considered to be the basis for off-terrain mobility [5, 6].

While a wheeled robot moving on the slopes that are covered with planetary regolith, the contact mechanics that act on the wheels by the terrain is complicated. The wheels may slip/skid in the longitudinal direction, or skid in the lateral direction. Slip velocity is defined as the difference between the theoretical circumference velocity and actual traveling velocity of a wheel. When the theoretical velocity is larger than the actual velocity, the difference is positive and it is called slip velocity. On the contrary, the difference is negative and its absolute value is called skid velocity. The ratio between the slip velocity and the theoretical velocity is called the slip ratio, while that between the skid velocity and the actual velocity is called skid ratio.

*Resrach supported by the National Natural Science Foundation of China (Grant No. 61005080/51275106), Foundation of Chinese State Key Laboratory of Robotics and Systems (Grant No. SKLRS201004B), Canada Research Chair Program, and the "111 Project" (Grant No. B07018).

L. Ding, H. Gao, Z. Deng, and J. Guo are with the State Key Laboratory of Robotics and System, Harbin Institute of Technology, Harbin 150001, Heilongjiang, China (e-mail: {liangding, gaohaibo, dengzq}@hit.edu.cn).

G. Liu and L. Ding (as a visiting scholar) are with the Department of Aerospace Engineering, Ryerson University, 350 Victoria Street, Toronto, Ontario M5B 2K3, Canada (e-mail: gjliu@ryerson.ca).

The wheels of planetary rovers will slip when they climb up deformable slopes in order to generate enough drawbar pull to balance the resistance caused by the gravity in the tangential surface of the slope. Intensive research has been carried out for WMRs considering the longitudinal slip of wheels. Ding et al. investigated on the interaction mechanics for different kinds of planetary rovers' wheels; the slip ratio was considered as the independent variable as it has critical influence on the drawbar pull, resistance moment and wheel sinkage [7]. The slip ratio is one of the most important state variables in the terramechanics equation for the wheels. Shibly et al. presented a simplified, closed-form version of mechanics model for a driven rigid wheel on the deformable terrain [8]. Lyasko [9] and Ding et al. [10] investigated the slip sinkage phenomena of vehicles and planetary WMRs moving in soft sand and developed models to predict the slip sinkage phenomena. The dynamics models of WMRs including the wheel slip are presented by Williams et al. [11], Balakrishna & Ghosal [12], and Yoshida & Hamano [13]. The slip ratio of planetary rovers' wheels could be measured using on-board sensors [14, 15] and compensated to follow the planned path [16-18].

On the other hand, a wheel will skid in the longitudinal direction in order to generate resistance force (negative drawbar pull) to balance the gravity component when a rover moves down the slopes. But the research on skid mechanics is rare. The process of skid is usually considered as the inverse process of slip, and the contact mechanics is the odd function of slip ratio, for instance, the tractive coefficient that determines the drawbar pull presented by Balakrishna & Ghosal [12]. However, Setterfield & Ellery noticed that the drawbar pull and resistance moment are antisymmetrical about the coordinate origin in the figures with slip ratio as the abscissa, according to both the primary experimental results obtained by Ding et al. [7], and the theoretical results predicted by Pacejka's "magic tyre formula" [19]. Thus they provided an equation to predict the skid mechanics according to the slip mechanics by using compensated terms [20]. Gao et al. deduced an empirical model [21] to predict the skid mechanics for planetary rovers' driving wheels based on the model for towed wheels of conventional terrestrial vehicles developed by Wong and Reece [22].

As intensive research has been carried out aiming at the mechanics of planetary rovers' wheels in the slip condition, to predict the skid mechanics of wheels according to the slip mechanics models is an effective approach. However, the relationship between the skid mechanics and slip mechanics is not clear yet. The contribution of this paper lies in the

experimental study, comparison, and semi-empirical modelling of skid mechanics versus slip mechanics.

The remained sections of this paper are organized as follows. Section II analyzes the problem of longitudinal slip and skid that could occur to a wheel on the slopes. Section III presents the experimental study based on a single-wheel testbed. Section IV proposes semi-empirical equations to predict the slip and skid mechanics. Finally, the conclusions are given in Section V.

II. Analysis of Slip versus Skid

A. Definition of Slip Ratio versus Skid Ratio

Let r denote the radius of a wheel, v, the traveling velocity in the longitudinal direction, ω, the angular velocity, then $r\omega$ is the theoretical circumference velocity.

If the theoretical velocity is larger than the longitudinal traveling velocity, a wheel slips and the slip ratio s is defined as:

$$s = (r\omega - v)/r\omega \quad (r\omega \geq v, 0 \leq s \leq 1) . \tag{1}$$

Or else, the theoretical velocity is smaller than the longitudinal traveling velocity, and the skid ratio s_d is defined as:

$$s_d = (v - r\omega)/v \qquad (r\omega \leq v, 0 \leq s_d \leq 1) . \tag{2}$$

In order to express the slip and skid of a wheel in a unified frame, when a wheel is skidding, the slip ratio could be defined as the minus value of skid ratio, i.e.,

$$s = -s_d = (r\omega - v)/v \qquad (r\omega \leq v, -1 \leq s \leq 0) , \tag{3}$$

If $r\omega = v$, $s = 0$, the wheel rotates and moves forward without slip or skid; if $s > 0$, the wheel slips; else if $s < 0$, the wheel skids, and $|s|$ is the skid ratio s_d, reflecting the degree of wheel skid. Generally, a driving wheel slips while climbing up slopes or accelerating; it skids while moving down slopes or decelerating, and a towed wheel also skids; while traversing on the flat terrain, the driving wheel usually has zero slip ratio or positive slip ratio with a small value.

The instantaneous center where the velocity is zero and the velocity distribution for wheels with different slip ratios could be found in Ref. [23]. If there is no slip or skid, the instantaneous center is the bottom-dead-center under the wheel. If a wheel slips, the instantaneous center is inside the wheel, and the velocity direction of the bottom-dead-center is opposite to that of the wheel center. If a wheel skids, the instantaneous center is outside of the wheel, and the velocity direction of the bottom-dead-center is the same as that of the wheel center.

Another method of defining the skid ratio that is denoted by s'_d is [22]:

$$s'_d = (v - r\omega)/r\omega \qquad (r\omega \leq v, 0 \leq s'_d < +\infty) . \tag{4}$$

According to Eqs. (2) and (4), one obtains:

$$\begin{cases} r\omega = (1 - s_d)v \\ (1 + s'_d)r\omega = v \end{cases} . \tag{5}$$

The relationship between s_d and s'_d is derived according to (5):

$$1 + s'_d = 1/(1 - s_d) . \tag{6}$$

For the wheels installed lugs with height of h, the shearing radius r_s should be used to calculate the slip ratio instead of r:

$$s = \begin{cases} (r_s\omega - v)/r_s\omega & (r_s\omega \geq v, 0 \leq s \leq 1) \\ (r_s\omega - v)/v & (r_s\omega \leq v, -1 \leq s \leq 0) \end{cases} . \tag{7}$$

where

$$r_s = r + \lambda_s h \ (0 \leq \lambda_s \leq 1) . \tag{8}$$

The value of λ_s could be calculated theoretically [24] or estimated by making sure the drawbar pull to be zero when the slip ratio is zero according to the experimental results [23].

B. Motion of Soil and Stresses Distribution under the Wheel

Fig. 1 shows the flow patterns of deformable soil beneath a driving rigid wheel under different circumstances. The angle $X_c = \pi/4 - \varphi/2$, where φ is the internal friction angle of the soil. There is a soil wedge moves forward in front of a locked wheel with 100% skid. If the wheel rotates without forward motion at 100% slip, the soil beneath it flows backward. There are generally two zones of soil flow beneath a driving wheel except for the extreme cases. In the front zone, the soil flows forward, and in the rear zone, it flows backward.

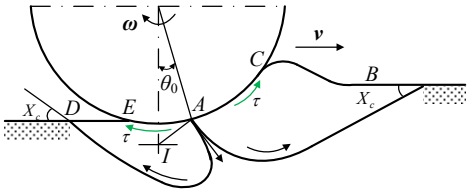

(a) $-1 \leq s < 0$, skid

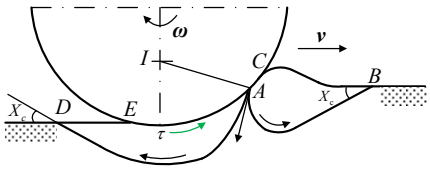

(b) $0 \leq s < 1$, slip

Figure 1. Flow pattern and bow wave under a driving wheel.

The stresses distribution beneath the driving wheels in the slip condition and the towed wheels without driving motors in the skid condition were measured by Onafeko et al [25]. The soil acts at the wheels in the form of continuous normal stress in the radial direction and the shearing stress in the tangential direction, which are denoted by $\sigma(\theta)$ and $\tau(\theta)$, respectively. The normal stress beneath a wheel in the slip and skid conditions are similar, as shown in Fig. 2, where W is the vertical load, T is the driving torque, and f_{DP} is the horizontal force that act at the wheel axle by the robot. The normal stress

increases from the entrance angle θ_1 and reaches the peak value at the angle of θ_m which is considered as the function of slip ratio, then it decreases to zero at the leaving angle of θ_2 (the angle where the normal stress is zero rather than where the wheel leaves the soil). The shear stress under a wheel in slip condition has the similar shape as the normal stress but with smaller value. However, the shear stress under a wheel in skid condition is quite different, as shown in Fig. 2 (b). At the transition point *A* in Fig. 1 (a), where two soil failure zones join each other having a corresponding transition angle θ_0, the shear stress is zero. From the angle of θ_1 to θ_0, the shear stress is positive, and it is negative from the angle of θ_0 to θ_2. Equations of predicting the stresses for driving wheels in the slip condition have been researched intensively [22, 24], but the research on stresses distribution for driving wheels in the skid condition is preliminary [21, 26].

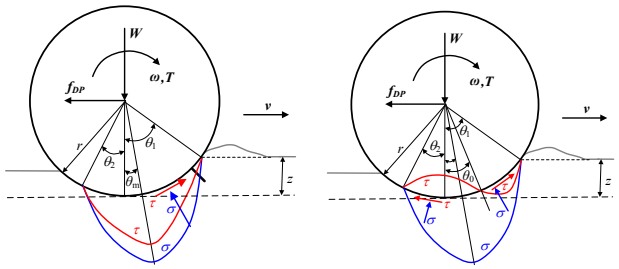

(a) Slip (b) Skid

Figure 2. Stresses distribution under a wheel.

B. *Climbing up (Slip) versus Moving down Slopes (Skid)*

Fig.3 shows the forces and moments that act on a driving wheel by the soil, vehicle body, and driving motor, while it climbs up a slope with slip or moves down a slope with skid, where F_N denotes the equivalent normal force, and F_{DP} denotes the drawbar pull.

The quasi-static equation of a wheel on the slope is:

$$\begin{cases} F_N = W\cos\alpha_{cl} \\ F_{DP} = W\sin\alpha_{cl} \\ M_{DR} = F_{DP}\cdot l + F_N\cdot e = T \end{cases}. \tag{9}$$

The dimension l is close to the radius r_s [7], and

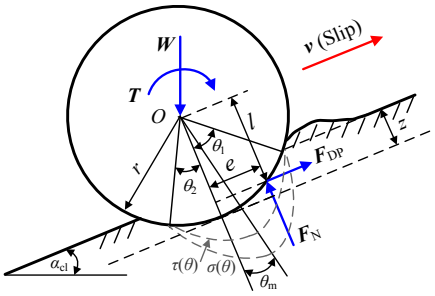

(a) Climbing up a slope with slip

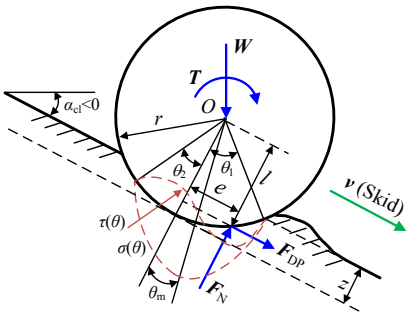

(b) Moving down a slope with skid

Figure 3. Forces and torque that act on a driving wheel.

$$T \approx F_{DP}\cdot r_s + F_N\cdot e\,, \tag{10}$$

$$F_{DP} \approx T/r_s - F_N\cdot e/r_s\,. \tag{11}$$

According to Eq. (9), if the slope angle α_{cl} is positive, the robots' wheels climb up the slopes with slip, and the drawbar pull which is equal to $W\sin\alpha_{cl}$ is also positive; or else, when the wheels move down a slope with a negative angle of α_{cl}, the drawbar pull is also negative, making it become a resistance force. Let $F_t = T/r_s$ to denote the traction force caused by the soil deformation while the wheel rotates with a driving torque of *T*. The component of $F_N\cdot e/r_s$ is the resistance caused by the soil, where e/r_s is the resistance coefficient denoted by λ_{RC}, reflecting the hindering effect to the wheel caused by the soil. The drawbar pull is the net force of the tractive and the resistance, and it can balance the force that act on the wheel's center by the robot.

Divide Eq. (11) by F_N, one obtains:

$$F_{DP}/F_N \approx T/(F_N r_s) - \lambda_{RC}\,. \tag{12}$$

Let $\lambda_{PC} = F_{DP}/F_N$, denoting the drawbar pull coefficient, and $\lambda_{TC} = T/(F_N r_s)$, denoting the tractive coefficient. According to Eq. (12), one obtains:

$$\lambda_{PC} \approx \lambda_{TC} - \lambda_{RC}\,, \tag{13}$$

The coefficient λ_{PC} is an index for evaluating the trafficability such as the slope climbing ability of a rover on the slopes. The relationship between λ_{PC} and α_{cl} is:

$$\lambda_{PC} = \frac{F_{DP}}{F_N} = \frac{W\sin\alpha_{cl}}{W\cos\alpha_{cl}} = \tan\alpha_{cl}\,. \tag{14}$$

Given the values of λ_{PC} versus slip ratio, the inclination angle of α_{cl} that a robot could climb up or move down can be calculated with Eq. (15):

$$\alpha_{cl} = \arctan(\lambda_{PC})\,. \tag{15}$$

III. Experimental Study with Single-wheel Testbed

A. Experimental Setup

The wheel-soil interaction testbed (Fig. 4) [7] developed by the authors' laboratory was used to test the slip and skid mechanics. The experimental wheel has dimensions of r157.35 mm (radius) × b165 mm (width); 30 lugs with heights of 15mm and 10mm, respectively, were installed to the wheels.

The planetary soil simulant HIT-LSS1 made from soft sand that was provided by Shanghai Academy of Spaceflight Technology was used. The soil parameters are: γ_s=15.73N/m^3, k_c=15.6 kPa/m^{n-1}, k_φ=2407.4 kPa/m^n, n=1.10, c=0.25 kPa, φ=31.9°, and K=9.7-13.1 mm [7].

The experimental setup is shown in Table I.

Figure 4. Testbed and expeimental wheel.

TABLE I. Design of Experiments

Group	Wheel	h (mm)	v (mm/s)	W (N)	s
1	Wh31	15	10	80	-1.0 to 0.6
2	Wh32	10			
3	Wh34	0			

B. Results

The measured data in the quasi-static state that fluctuate with the entering and leaving of the wheel lugs were used. A Matlab program was developed to draw the curves of the original data versus time, calculate the mean value and standard deviation. During experiment, the slip ratios were calculated using the maximum radius of r+h, and then it was amended by finding the value of λ_s, which are 0.75 and 0.65 for the wheels of Wh31 and Wh32, respectively. The experimental skid ratios were calculated using the shearing radius r_s. Fig. 5 shows the experimental results of wheel sinkage, driving torque, and drawbar pull.

The shape of the curve for wheel sinkage looks like a basin. If the slip ratio ranges from -0.2 (-0.3) to 0.1, the wheel sinkage has small variation. While it increases rapidly if the skid ratio is larger than 0.2 (03), or the slip ratio is larger than 0.1. The wheel sinkage for the wheel with lugs of 15mm in height is smaller due to the supporting effect of lugs. The difference is about 4 mm if the skid ratio is larger than 0.3. The sinkage for wheel Wh31 is smaller when the slip ratio ranges from 0 to 0.3 comparing with that for Wh34. But the wheel sinkage of Wh31 is larger if the slip ratio is larger than 0.3, as the soil is digging and removing more severely by the higher wheel lugs.

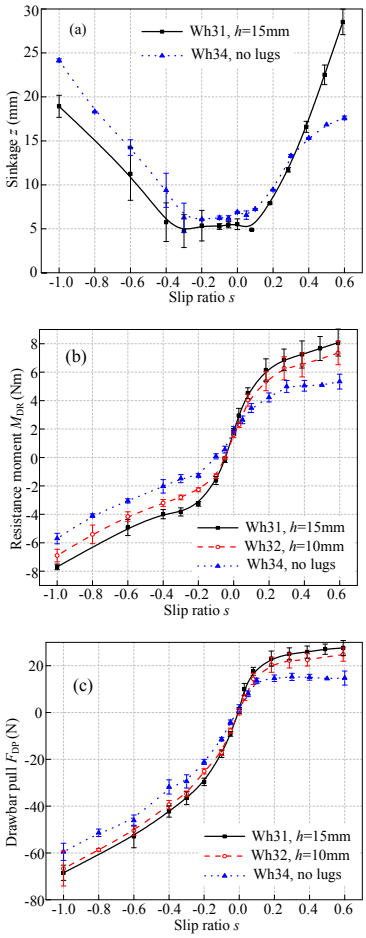

Figure 5. Experimental results under condition of slip versus skid.

The driving torque increases from a smallest negative value when the slip ratio is -1 to a maximum positive value when the slip ratio is 0.6. The driving torque is no zero when there is no slip or skid, but has an approximate value of 1.5-2.0 Nm. The absolute values of M_{DR} when the slip ratio is -1 are close to those with slip ratio of 0.6. Therefore, it is reasonable to design the motor and reduction mechanism of a wheel according to the slip mechanics

When the slip ratio increases from 0 to 0.2, the drawbar pull increases rapidly, then it increases slowly if the slip ratio ranges from 0.2 to 0.6. With the increase of skid ratio, the absolute values of the drawbar pull increase rapidly. With the increase of slip ratio or skid ratio, the wheel sinkage increases to generate larger resistance force. The resistance force counteracts the tractive force to decrease the drawbar pull when a wheel sips. But for a skid wheel, the resistance force is in the same direction as the tractive force, both of which are resistance force increasing with skid ratio.

All the measured results are not symmetrical. The driving torque is influenced by the positive value when the slip ratio is zero. The drawbar pull is mainly influenced by the resistance force, which decrease the value of drawbar pull when it slips, and increase the absolute value of drawbar pull when it skids.

C. Analysis of the relative performances

In order to understand the slip versus skid mechanics better, the relative indices which are shown in Fig. 6 should be analyzed.

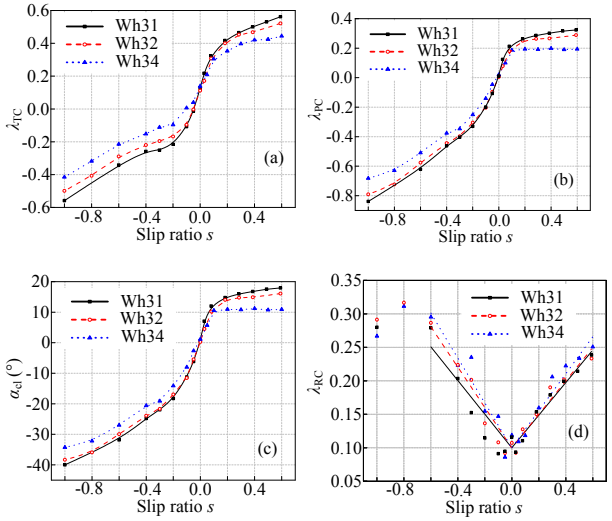

Figure 6. Relative indices of wheels in slip and skid condition.

The tractive coefficient λ_{TC} ranges approximately [-0.6, 0.6], [-0.5, 0.5], and [-0.4, 0.4] for Wh31, Wh32 and Wh34, respectively. But when the tractive coefficient λ_{TC} is zero, the slip ratios range approximately from -0.1 to -0.05. The pull coefficient λ_{PC} ranges approximately [-0.8, 0.3] for wheels with lugs and [-0.7, 0.2] for wheel Wh34 without lugs.

The wheels are not recommended to work at the slip ratios larger than 0.6 as the wheel sinkage increases more rapidly beyond this value [7]. When the slip ratio is 0.6, the robot installing the wheels with lugs could climb up the maximum slopes of near 20 degrees, but it could moves down slopes of near 40 degrees when the skid ratio is -1. If a robot with the lugged wheels moves down the slopes of near 20 degrees, the skid ratio is only about 0.2, much smaller than the slip ratio while climbing up a slope with the same angle. As a result, it is much easier for a robot moving down a slope than climbing up a slope with the same angle. The slip ratio of [-0.6, 0.6] could cover most of the working spectrum of a robot.

The resistance coefficient λ_{RC} has the smallest value of approximately 0.1 when the slip ratio is zero, and it increases linearly to approximately 0.25 when the slip ratio is 0.6, and near 0.30 when the skid ratio is 0.6. Eq. (16) is proposed to estimate λ_{RC} for different wheels. Table II show the results of the parameters in Eq. (16) obtained from data fitting. The values of b_{RC}[a] which are estimated from data fitting for different wheels are close to 0.1, so that b_{RC} were set to be 0.1 for all the wheels. The resistance coefficient is influenced by the coupled effects of slip ratio, wheel sinkage and wheel lugs. The slip ratio influences the resistance coefficient primarily by influencing the wheel sinkage, but the wheel in the skid condition has larger λ_{RC} comparing with the slip condition when the wheel sinkages are the same. The wheel lugs also influence λ_{RC}. For example, when the slip ratio is 0.6, the sinkage for wheel Wh31 is much larger than that for Wh34, but the resistance coefficient of Wh31 is smaller. That's because the wheel sinkage is partially caused by the digging and removing of the lugs that cannot generate resistance compaction force. The increasing slope of λ_{RC} in Eq. (16) for a wheel with higher lugs is larger.

$$\lambda_{RC} = \begin{cases} k_{RC2}s + b_{RC} & (0 \le s \le 0.6) \\ k_{RC1}s_d + b_{RC} & (0 \le s_d \le 0.6) \end{cases}. \tag{16}$$

TABLE II. IDENTIFIED PARAMETERS FOR EQ. (16)

Wheel	k_{RC1}[a]	b_{RC}[a]	k_{RC1}[b]	b_{RC}[b]	k_{RC2}[b]
Wh34	0.270	0.103	0.335	0.10	0.276
Wh32	0.241	0.103	0.301		0.250
Wh31	0.252	0.096	0.251		0.243

a. b_{RC} is identified by data fitting; b. b_{RC} is designated to be 0.10.

IV. SEMI-EMPIRICAL MODELLING

Seen from Fig. 6, the wheel sinkage, resistance moment and drawbar pull can be fitted with three pieces of linear functions. By analyzing the function parameters, one can find the relationship between the slip mechanics and skid mechanics, in order to estimate the skid mechanics according to the slip mechanics.

A. Piecewise linear function

The wheel sinkage can be predicted with Eq. (17):

$$z = \begin{cases} k_z s + b_z \, (s_{z1} \le s \le s_{z2}) \\ k_{z1} s + b_{z1} \, (-1 \le s \le s_{z1}) \\ k_{z2} s + b_{z2} \, (s_{z2} \le s \le 1) \end{cases} \tag{17}$$

The sinkage corresponding to the slip ratio of [-1.0, -0.4], [-0.3, 0.1], and [0.2, 0.6] were used to identify the function parameters, respectively. The data fitting results is shown in Fig. 7 (a) and the parameters are listed in Table III. If the slip ratios are s_{z1} or s_{z2}, the following equations hold:

$$\begin{cases} k_z s_{z1} + b_z = k_{z1} s_{z1} + b_{z1} \\ k_z s_{z2} + b_z = k_{z2} s_{z2} + b_{z2} \end{cases} \tag{18}$$

The transitional slip ratios are obtained by solving Eq. (18):

$$\begin{cases} s_{z1} = (b_{z1} - b_z)/(k_z - k_{z1}) \\ s_{z2} = (b_{z2} - b_z)/(k_z - k_{z2}) \end{cases} \tag{19}$$

TABLE III. FITTED PARAMETERS FOR WHEEL SINKAGE

Wheel	k_z	b_z	k_{z1}	b_{z1}	k_{z2}	b_{z2}	s_{z1}	s_{z2}
Wh31	0.7	5.3	-21.6	-2.4	50.9	-2.2	-0.35	0.16
Wh34	2.3	6.7	-24.2	-0.4	19.9	6.5	-0.27	0

The value of k_z is much smaller than the absolute values of k_{z1} and k_{z2}. $|k_{z1}|$ and k_{z2} for the wheel without lugs are close, but k_{z2} is twice as $|k_{z1}|$ for Wh31 with lugs of 15mm in height. Also, the values of $|k_{z1}|$ for wheels Wh34 and Wh31 are close. The slip-sinkage caused by soil digging effect of wheel lugs is obvious.

The functions of predecting the resistance moment and drawbar pull are:

$$M_{\mathrm{DR}}=\begin{cases}(k_{\mathrm{DR}}s+b_{\mathrm{DR}})F_{\mathrm{N}}r_{\mathrm{s}} & (s_{\mathrm{DR1}}\le s\le s_{\mathrm{DR2}})\\ (k_{\mathrm{DR1}}s+b_{\mathrm{DR1}})F_{\mathrm{N}}r_{\mathrm{s}} & (-1\le s\le s_{\mathrm{DR1}})\\ (k_{\mathrm{DR2}}s+b_{\mathrm{DR2}})F_{\mathrm{N}}r_{\mathrm{s}} & (s_{\mathrm{DR2}}\le s\le 1)\end{cases} \tag{20}$$

$$F_{\mathrm{DP}}=\begin{cases}k_{\mathrm{DP}}sF_{\mathrm{N}} & (s_1\le s\le s_2)\\ (k_{\mathrm{DP1}}s+b_{\mathrm{DP1}})F_{\mathrm{N}} & (s\le s_1)\\ (k_{\mathrm{DP2}}s+b_{\mathrm{DP2}})F_{\mathrm{N}} & (s_2\le s)\end{cases} \tag{21}$$

And the transitional slip ratios could be calculated with the following equations:

$$\begin{cases}s_{\mathrm{DR1}}=(b_{\mathrm{DR1}}-b_{\mathrm{DR}})/(k_{\mathrm{DR}}-k_{\mathrm{DR1}})\\ s_{\mathrm{DR2}}=(b_{\mathrm{DR2}}-b_{\mathrm{DR}})/(k_{\mathrm{DR}}-k_{\mathrm{DR2}})\end{cases} \tag{22}$$

$$\begin{cases}s_{\mathrm{DP1}}=b_{\mathrm{DP1}}/(k_{\mathrm{DP}}-k_{\mathrm{DP1}})\\ s_{\mathrm{DP2}}=b_{\mathrm{DP2}}/(k_{\mathrm{DP}}-k_{\mathrm{DP2}})\end{cases} \tag{23}$$

The resistance moment and drawbar pull corresponding to the slip ratios of [-1.0, -0.2], [-0.1, 0.1], and [0.2, 0.6] were used to identify the function parameters in Eqs. (20) and (21), respectively. The results are shown in Tables IV and V. The approximate average normal force is 85 N. The data fitting results are shown in Fig. 7 (b) and (c).

The parameters of k_{DR1} are close for different wheels. The value of k_{DR2} for the wheel without lugs is much smaller than its k_{DR1}, whereas the values of k_{DR2} are a bit smaller than the corresponding k_{DR1} for the wheels with lugs. The values of b_{DR} for different wheels are also close, but the values of k_{DR} for the lugged wheels are much larger than that for the smooth wheel.

The values of k_{DP1} for all the wheels are close, but the values of k_{DP} and k_{DP2} are much larger for the wheels with lugs comparing with those for the wheel Wh34.

TABLE IV. FITTED PARAMETERS FOR RESISTANCE MOMENT

Wheel	k_{DR}	b_{DR}	k_{DR1}	b_{DR1}	k_{DR2}	b_{DR2}	s_{DR1}	s_{DR2}
Wh31	2.61	0.13	0.39	-0.14	0.32	0.38	-0.13	0.12
Wh32	2.21	0.11	0.41	-0.07	0.32	0.33	-0.11	0.13
Wh34	1.33	0.13	0.39	0.01	0.16	0.28	-0.14	0.14

TABLE V. FITTED PARAMETERS FOR DRAWBAR PULL

Wheel	k_{DP}	k_{DP1}	b_{DP1}	k_{DP2}	b_{DP2}	s_{DP1}	s_{DP2}
Wh31	2.34	0.56	-0.26	0.13	0.25	-0.15	0.11
Wh32	2.04	0.60	-0.22	0.12	0.22	-0.15	0.12
Wh34	1.46	0.56	-0.16	0	0.18	-0.18	0.12

B. Prediction of Skid Mechanics Based on Slip Mechanics

There exist many models in the literatures that predict the slip mechanics for WMRs [8, 13, 24]. It is useful to estimate the skid mechanics according to the slip mechanics. As most of the wheels for planetary rovers have lugs to enhance the tractive performance, so that the lugged wheels are the main concern.

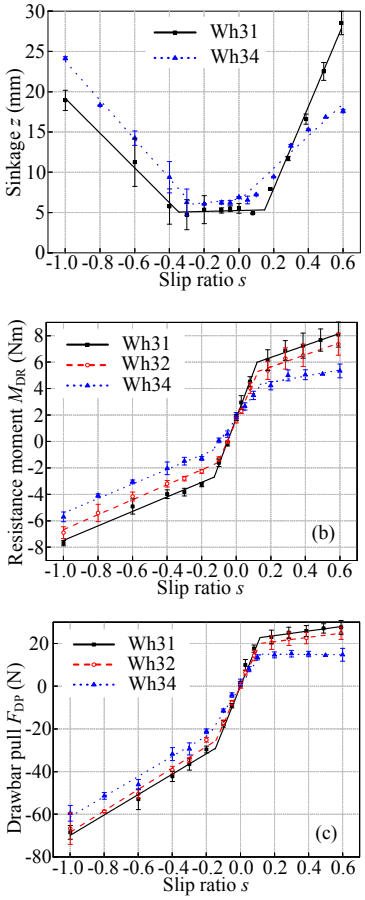

Figure 7. Comparison of predicted and experimental results.

The wheel sinkage z, tractive coefficient λ_{TC} and resistance coefficient λ_{RC} could be estimated using the terramechanics models [8, 24] for wheels in the slip condition. In order to reflect the antisymmetrical property of slip and skid, and predict the skid mechanics with slip mechanics, we propose the following equations for the prediction of tractive coefficient and resistance moment for a wheel with skid ratio of s_{d} (or slip ratio of s=-s_{d}) based on analysis of the results in Table IV:

$$\lambda_{\mathrm{TC}}(s=-s_{\mathrm{d}})=-\lambda_{\mathrm{TC}}(s_{\mathrm{d}})+2\lambda_{\mathrm{TC0}}\ (-1\le s\le 0) \tag{26}$$

$$\begin{aligned}M_{\mathrm{DR}}(s=-s_{\mathrm{d}})&=T(s=-s_{\mathrm{d}})\\ &=(-\lambda_{\mathrm{TC}}(s_{\mathrm{d}})+2\lambda_{\mathrm{TC0}})F_{\mathrm{N}}r_{\mathrm{s}}\quad(-1\le s\le 0)\end{aligned} \tag{27}$$

where λ_{TC0} has the same meaning as b_{DR}, with values of 0.13 for Wh31 and 0.11 for Wh32.

According to the results in Table II, we obtain:

$$\lambda_{\mathrm{RC}}(s=-s_{\mathrm{d}})\approx-\lambda_{\mathrm{RC}}(s_{\mathrm{d}})\ (-1\le s\le 0) \tag{28}$$

Substitute Eqs. (26) and (28) into to Eq. (13), one obtains:

$$\begin{aligned}F_{\mathrm{DP}}(s=-s_{\mathrm{d}})&=[\lambda_{\mathrm{TC}}(s)-\lambda_{\mathrm{RC}}(s)]F_{\mathrm{N}}\\ &\approx(-\lambda_{\mathrm{TC}}(s_{\mathrm{d}})-\lambda_{\mathrm{RC}}(s_{\mathrm{d}})+2\lambda_{\mathrm{TC0}})F_{\mathrm{N}}\quad(-1\le s\le 0)\end{aligned} \tag{29}$$

According to the results in Tables II and IV for the wheel in slip condition, Fig. 8 is drawn. The errors while predicting the skid mechanics are acceptable.

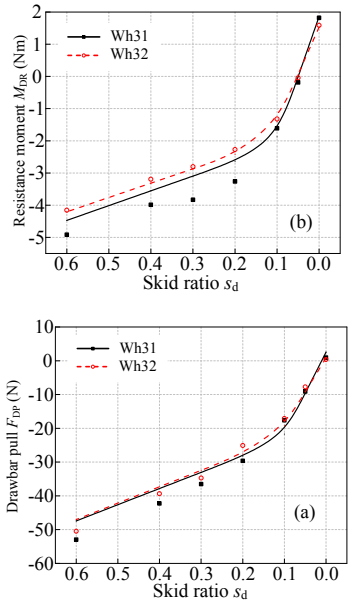

Figure 8. M_{DR} and F_{DP} in skid condition predicted with slip mechanics.

V. Conclusions and Future Work

The skid mechanics is antisymmetrical from the slip mechanics in that: (1) the resistance moment is not zero where there is no slip or skid; (2) the drawbar pull is the summation of resistance force and tractive force; the latter does not change its direction whereas the latter changes its direction. The slip versus skid mechanics could be predicted with piecewise linear functions. Equations of estimating skid mechanics according to the slip mechanics by considering the antisymmetrical characteristics of resistance moment and drawbar pull are proposed and verified by experiments. The slip and skid mechanics models will be applied to the modelling and control of planetary rovers in the future.

References

[1] NASA JPL, "Mars exploration rover," http://marsrovers.jpl.nasa.gov/home/index.html , Accessed on Jan. 9, 2013.

[2] NASA, "Mars Science Laboratory, Curiosity: Could Mars Have Once Harbored Life?" http://www.nasa.gov/mission_pages/msl/ index.html , Accessed on Jan. 9, 2013.

[3] ESA, "Robotic exploration of Mars: ExoMars," http://www.esa.int/SPECIALS/ExoMars/SEM10VLPQ5F_0.html, Accessed on Jan. 9, 2013.

[4] C. R. Neal, "The moon 35 years after Apollo: what's left to learn?," *Chemie der Erde – Geochemistry*, vol. 69, no. 1, pp. 3–43, 2009.

[5] L. Ding, Z. Q. Deng, H. B. Gao, K. Nagatani, and K. Yoshida, "Planetary rovers' wheel-soil interaction mechanics: new challenges and applications for wheeled mobile robots," *Journal of Intelligent Service Robotics*, vol. 4, no. 1: pp. 17–38, 2011.

[6] A. Ellery, "Environment-robot interaction–the basis for mobility in planetary micro-rovers," Robotics and Autonomous Systems, vol. 51, no. 1, pp. 29–39, 2005.

[7] L. Ding, Z. Q. Deng, H. B. Gao, K. Nagatani, K. Yoshida, "Experimental study and analysis on driving wheels' performance for planetary exploration rovers moving in deformable soil," *Journal of Terramechanics*, vol. 48, no. 1, pp. 27–45, 2011.

[8] H. Shibly, K. Iagnemma, and S. Dubowsky "An equivalent soil mechanics formulation for rigid wheels in deformable terrain, with application to planetary exploration rovers," *Journal of Terramechanics*, vol. 42, no. 1, pp. 1–13, 2005.

[9] M. Lyasko, "LSA model for sinkage predictions," *Journal of Terramechanics,* vol. 47, no. 1, pp. 1–9, 2010.

[10] L. Ding, H. B. Gao, Z. Q. Deng, J. G. Tao, "Wheel slip-sinkage and its prediction model of lunar rover," *Journal of Central South University of Technology*, vol. 17, no. 1, pp. 129–135, 2011.

[11] R. L. Williams II, B. E. Carter, P. Gallina, and G. Rosati, "Dynamic model with slip for wheeled omnidirectional robots," *IEEE Transactions on Robotics and Automation*, vol. 18, no. 3, pp. 285–293, 2002.

[12] R. Balakrishna and A. Ghosal, "Modeling of slip for wheeled mobile robots," I*EEE Transactions on Robotics and Automation*, vol. 11, no. 1, pp.126–132, 1995.

[13] K. Yoshida and H. Hamano, "Motion dynamics of a rover with slip-based traction model," in *Proc. IEEE International Conference on Robotics and Automation*, Washington, DC, USA, pp. 3155–3160, 2002.

[14] G. Reina, L. Ojeda, A. Milella, J. Borenstein. Wheel slippage and sinkage detection for planetary rovers. *IEEE/ASME Transactions on Mechatronics*, vol. 11, no. 2, pp. 185–195, 2006.

[15] M. Maimone, Y. Cheng, and L. Matthies., "Two years of visual odometry on the Mars exploration rovers," *Journal of Field Robotics*, vol. 24, no. 3, pp. 169–186, 2007.

[16] Y. Cheng, D. S. Clouse, and M. Bajracharya, "Slip compensation for a Mars rover," in *Proc. IEEE/RSJ International Conference onIntelligent Robots and Systems*, Edmonton, Alberta, Canada, pp. 2806–2813, 2005.

[17] D. M. Helmick, S. I. Roumeliotis, and Y. Cheng, "Slip-compensated path following for planetary exploration rovers," *Advanced Robotics*, vol. 20, no. 11, pp. 1257-1280, 2006.

[18] G .Ishigami, K. Nagatani, and K. Yoshida, "Path Following Control with Slip Compensation on Loose Soil for Exploration Rover," in: *Proc. IEEE/RSJ International Conference on Intelligent Robots and Systems*, Beijing, China, 2006, pp. 5552–5557.

[19] H. B. Pacejka and E. Bakker, "The magic formula tyre model," *Vehicle System Dynamics*, vol. 21, no. sup 001, pp. 1–18, 1992.

[20] T.P. Setterfield, and A. Ellery, "Terrain response estimation using an instrumented rocker-bogie mobility system," *IEEE Transactions on Robotics*, vol. 29, no. 1, pp. 172–188, Feb. 2013.

[21] H. B. Gao, J. L. Guo, L. Ding, et al., "Longitudinal skid model for wheels of planetary exploration rovers based on terramechanics," *Journal of Terramechanics*, submitted for publication.

[22] J. Y. Wong, and A. R. Reece, "Prediction of rigid wheel performance based on analysis of soil-wheel stresses, part II: performance of towed rigid wheels," *Journal of Terramechanics*, vol. 4, no. 2, pp. 7–25, 1967.

[23] L. Ding, H. B. Gao; Z. Q. Deng, K. Yoshida and K. Nagatani, "Slip ratio for lugged wheel of planetary rover in deformable soil: definition and estimation," in *Proc. IEEE/RSJ International Conference on Intelligent Robots and Systems*, St. Louis, MO, USA, 2009, pp. 3343–3348.

[24] L. Ding, Z. Q. Deng, H. B. Gao, J. G. Tao, K. D. Iagnemma and G. Liu, "Terramechanics model of driving wheels for planetary WMRs moving on deformable soil considering multiple effects," *Journal of Field Robotics*, submitted for publication.

[25] O. Onafeko and A. R. Reece, "Soil stresses and deformations beneath rigid wheels," *Journal of Terramechanics*, vol. 4, no. 1, pp. 59-80, 1967.

[26] J. Y. Wong, and A. R. Reece, "Prediction of rigid wheel performance based on analysis of soil-wheel stresses, part II: performance of towed rigid wheels," *Journal of Terramechanics*, vol. 4, no. 2, pp. 7-25, 1967.